Fibrillin-1 regulates the bioavailability of TGFβ1

Shazia S. Chaudhry,[1,2] Stuart A. Cain,[1] Amanda Morgan,[1] Sarah L. Dallas,[3] C. Adrian Shuttleworth,[1] and Cay M. Kielty[1,2]

[1]Wellcome Trust Centre for Cell-Matrix Research and [2]UK Centre for Tissue Engineering, Faculty of Life Sciences, University of Manchester, Manchester M13 9PT, England, UK
[3]Department of Oral Biology, School of Dentistry, University of Missouri, Kansas City, MO 64108

We have discovered that fibrillin-1, which forms extracellular microfibrils, can regulate the bioavailability of transforming growth factor (TGF) β1, a powerful cytokine that modulates cell survival and phenotype. Altered TGFβ signaling is a major contributor to the pathology of Marfan syndrome (MFS) and related diseases. In the presence of cell layer extracellular matrix, a fibrillin-1 sequence encoded by exons 44–49 releases endogenous TGFβ1, thereby stimulating TGFβ receptor–mediated Smad2 signaling. This altered TGFβ1 bioavailability does not require intact cells, proteolysis, or the altered expression of TGFβ1 or its receptors. Mass spectrometry revealed that a fibrillin-1 fragment containing the TGFβ1-releasing sequence specifically associates with full-length fibrillin-1 in cell layers. Solid-phase and BIAcore binding studies showed that this fragment interacts strongly and specifically with N-terminal fibrillin-1, thereby inhibiting the association of C-terminal latent TGFβ-binding protein 1 (a component of the large latent complex [LLC]) with N-terminal fibrillin-1. By releasing LLC from microfibrils, the fibrillin-1 sequence encoded by exons 44–49 can contribute to MFS and related diseases.

Introduction

Fibrillin microfibrils of the ECM, which associate with elastic fibers, are implicated in the regulation of TGFβ in large latent complexes (LLCs; for review see Ramirez et al., 2004; Kielty, 2006). Fibrillin-1 is a multidomain cysteine-rich glycoprotein containing 43 calcium-binding EGF (cbEGF)–like domains and 78 cysteine-containing TB motifs (Pereira et al., 1993). Fibrillin-1 mutations cause the heritable disorder Marfan syndrome (MFS) with severe cardiovascular, skeletal, ocular, and lung manifestations (for review see Robinson et al., 2006).

Enhanced TGFβ signaling is a major contributor to the pathology of MFS. A model has been proposed in which fibrillin-1 mutations perturb the normal microfibril regulation of latent TGFβ and, thereby, contribute to MFS pathogenesis (for review see Dietz et al., 2005). The clinically overlapping conditions, Loeys-Dietz aortic aneurysm syndrome, familial thoracic aortic aneurysms and dissections, and marfanoid craniosynostoses are also caused by enhanced TGFβ signaling but, in these cases, are caused by cytoplasmic kinase mutations in TGFβ receptor (TGFβR) I or II (Mizuguchi et al., 2004; Loeys et al., 2005, 2006; Ades et al., 2006; Matyas et al., 2006; Singh et al., 2006).

Correspondence to Cay M. Kielty: cay.kielty@manchester.ac.uk

Abbreviations used in this paper: ANOVA, analysis of variance; cbEGF, calcium-binding EGF; HDF, human dermal fibroblast; LAP, latency-associated propeptide; LLC, large latent complex; LTBP, latent TGFβ-binding protein; MFS, Marfan syndrome; SLC, small latent complex; TGFβR, TGFβ receptor; TSP-1, thrombospondin-1.

Mouse MFS models have revealed that enhanced TGFβ activity in fibrillin-1 haploinsufficient mice leads to primary developmental failures, including distal alveolar septation (Neptune et al., 2003), and, in heterozygous mutant mice, leads to mitral valve defects (Ng et al., 2004). Haploinsufficiency triggers secondary cellular events that result in intimal hyperplasia and adventitial inflammation with TGFβ involvement as well as aortic failure (for review see Dietz et al., 2005). Losartan, an angiotensin II blocker that lowers blood pressure and leads to the clinically relevant attenuation of TGFβ signaling, prevented aortic aneurysm in a mouse MFS model (Habashi et al., 2006). Tight-skin mice have enhanced TGFβ activity and sclerosis as a result of an internal fibrillin-1 duplication and a larger than normal secreted protein (Siracusa et al., 1996; Menon et al., 2006).

TGFβ is secreted from cells as a dimeric small latent complex (SLC) comprising noncovalently associated latency-associated propeptide (LAP) and active TGFβ and/or as a large LLC comprising SLC bound covalently to a latent TGFβ-binding protein (LTBP) through a TB motif (for reviews see Annes et al., 2003; Hyytiäinen et al., 2004). Only LTBP-1 and -3 bind TGFβ strongly. It has been proposed that by interacting with LLC, fibrillin microfibrils may act as a growth factor highway in tissues (for review see Ramirez et al., 2004). LTBPs are structurally related to fibrillins (for review see Sinha et al., 1998). LTBP-1 but not LTBP-3 can bind in vitro to fibrillin-1 (Isogai et al., 2003). This interaction involves three C-terminal domains

The Journal of Cell Biology, Vol. 176, No. 3, January 29, 2007 355–367
http://www.jcb.org/cgi/doi/10.1083/jcb.200608167

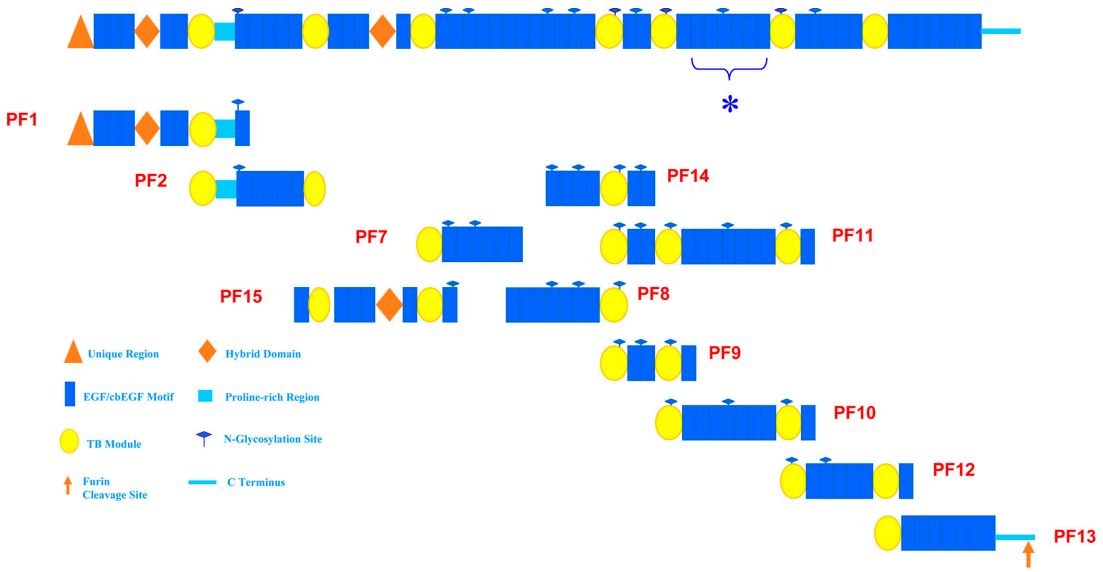

Figure 1. **Human recombinant fibrillin-1 fragments spanning full-length fibrillin-1.** Fibrillin-1 fragments were cloned into pCEP-His, expressed in 293-EBNA cells, and purified as previously described (Cain et al., 2005, 2006; Marson et al., 2005). The asterisk denotes the six cbEGF-like domains in fragments PF10 and PF11 that regulate TGFβ.

of LTBP-1 and four N-terminal domains of fibrillin-1. LTBP-1 is an associated but not an integral component of microfibrils (Isogai et al., 2003; Cain et al., 2006), and it colocalizes with fibrillin microfibrils in some tissues (Dallas et al., 2000; Isogai et al., 2003). The prodomain of another TGFβ superfamily member, BMP-7, can bind an N-terminal fibrillin-1 fragment in vitro (Gregory et al., 2005).

Activation of TGFβ, a potent growth factor that regulates cell proliferation, migration, differentiation, and survival, is normally tightly regulated. However, physiological activation mechanisms leading to receptor signaling are incompletely understood. They may involve LTBP-1–mediated proteolytic release, thrombospondin-1 (TSP-1) competition with SLC, integrin presentation, pH changes, and reactive oxygen species (for reviews see Annes et al., 2003; Hyytiäinen et al., 2004; Young and Murphy-Ullrich, 2004; Fontana et al., 2005; Gomez-Duran et al., 2006). Autoantibodies to a fibrillin-1 proline-rich region induce fibroblast activation possibly by releasing sequestered TGFβ1 from microfibrils (Zhou et al., 2005). BMP-1 also controls TGFβ1 activation by cleaving LTBP-1 (Ge and Greenspan, 2006). Once activated, TGFβ binding to TGFβRI and II heterodimers leads to the phosphorylation of TGFβRI, which, in turn, phosphorylates signaling proteins Smad2 and Smad3 (for reviews see Shi and Massague, 2003; Feng and Derynck, 2005). Smad2 and Smad3 phosphorylation allows association with Smad4, nuclear translocation, and specific gene activation or repression.

We have discovered that in the presence of cells, a specific fibrillin-1 sequence encoded by exons 44–49 regulates the bioavailability of endogenous TGFβ1, thereby stimulating Smad2 signaling. Fibrillin-1–mediated TGFβ release from ECM does not require intact cells, proteolysis, or changes in the expression of TGFβ or its receptors. A fibrillin-1 fragment containing the TGFβ-regulating sequence specifically binds deposited fibrillin-1 in the insoluble cell layer through a strong interaction with the fibrillin-1 N-terminal region. This interaction, which directly inhibits the association of C-terminal LTBP-1 with fibrillin-1, can thus release LLC from microfibrils. This novel mechanism is likely to contribute to TGFβ dysregulation in MFS and related diseases and in acquired fibrotic disorders.

Results

Regulation of TGFβ signaling by a specific fibrillin-1 sequence

Our first step was to determine whether fibrillin-1 could stimulate the Smad2 pathway. Recombinant fragments encompassing

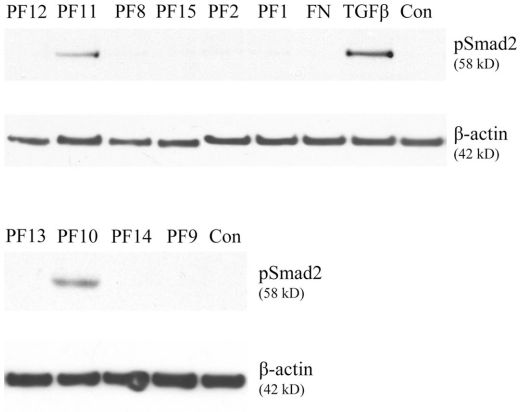

Figure 2. **PF10 and PF11 stimulate Smad2 phosphorylation.** 0.15 μM of fibrillin-1 recombinant fragments PF1, PF2, PF8, PF9, PF10, PF11, PF12, PF13, PF14, and PF15 were tested for their ability to stimulate Smad2 phosphorylation. The negative control (Con) contained no added proteins. 4 nM of human recombinant TGFβ1, which stimulates Smad2 signaling, was a positive control. 0.15 μM of human plasma fibronectin (FN) was an additional control. Only PF10 and PF11 stimulated Smad2 signaling. This experiment was repeated three times with similar results.

full-length human fibrillin-1 (Fig. 1) were tested for their ability to induce Smad2 phosphorylation in human dermal fibroblasts (HDFs) that were cultured in serum-free conditions. Overlapping fragments PF10 and PF11 but not overlapping fragments PF8, PF9, PF12, and PF14 were found to stimulate Smad2 signaling (Fig. 2). No other fibrillin-1 fragments or human plasma fibronectin stimulated Smad2 phosphorylation (Fig. 2). Thus, the Smad2-stimulating effect was mapped to a specific fibrillin-1 sequence of six contiguous cbEGF-like domains that are encoded by exons 44–49 (Fig. 1, asterisk). Similar results were obtained using the mouse osteoblast cell line 2T3 (unpublished data). ELISA assays revealed that purified PF10 alone contained no active TGFβ (R^2 0.9988), and repeated mass spectrometry failed to detect any trace of LAP or TGFβ tryptic peptides in purified PF10 preparations (Cain et al., 2006; unpublished data).

Stimulation of Smad2 signaling by fibrillin-1 requires TGFβRI and II

TGFβ1 signals through a heteromeric complex of TGFβRI and II, which have serine/threonine kinase activity (for reviews see Shi and Massague, 2003; Feng and Derynck, 2005). We investigated whether the Smad2 signaling effects of fibrillin-1 fragments PF10 or PF11 were exerted through these receptors (Fig. 3). First, an antibody that blocks TGFβRII was used in cell signaling inhibition assays. In the presence of the inhibitory TGFβRII antibody, there was no Smad2 stimulation by PF10 (Fig. 3 A) or PF11 (not depicted). The TGFβRII-inhibiting antibody also blocked TGFβ1-induced Smad2 phosphorylation (Fig. 3 A).

A chemical inhibitor, [3-(pyridin-2-yl)-4-(4-quinonyl)]-1H-pyrazole, which is an ATP-competitive inhibitor of TGFβRI kinase (Sawyer et al., 2003), was then used in Smad2 signaling inhibition assays to ascertain whether TGFβRI was also involved

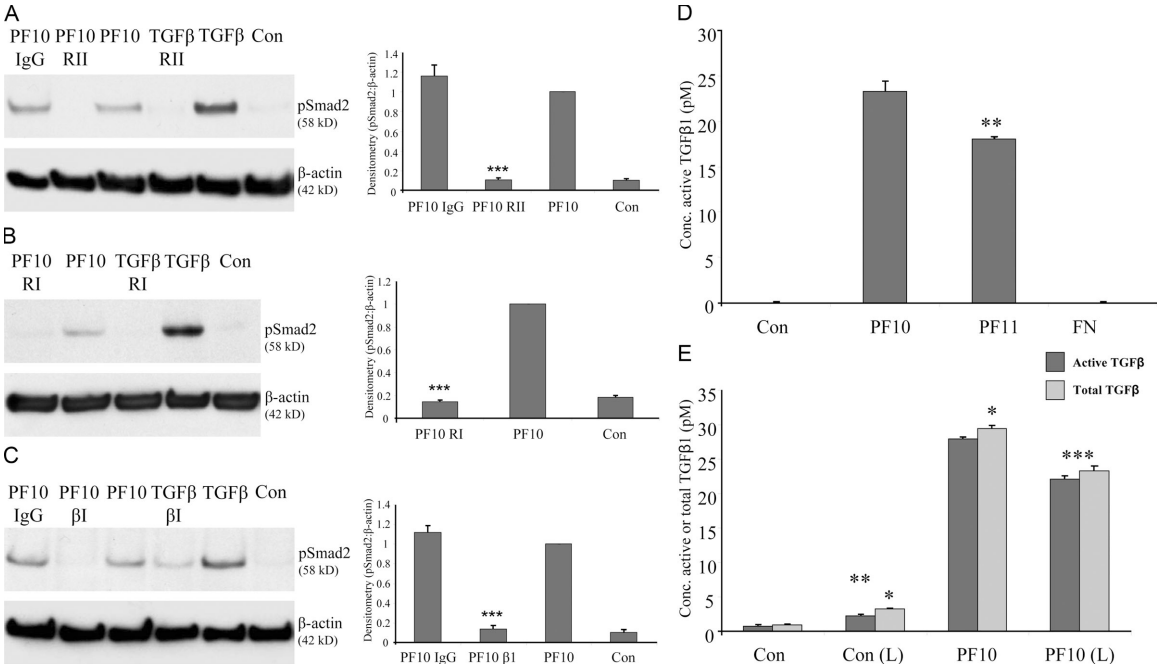

Figure 3. **PF10 stimulates Smad2 phosphorylation through TGFβRs and activates TGFβ1.** (A) When TGFβRII was blocked using 15 μg/ml of a neutralizing antibody (RII), Smad2 phosphorylation caused by PF10 stimulation was ablated (***, $P < 0.0001$ by *t* test in comparison with the PF10 control). A control antibody that has no inhibitory effect on the TGFβ pathway (IgG) confirmed that ablation of PF10 stimulation was caused by the specific TGFβRII antibody. (B) PF10 stimulation of Smad2 signaling was ablated when TGFβRI was blocked using a TGFβRI kinase chemical inhibitor (RI; ***, $P < 0.0001$ by *t* test in comparison with the PF10 control). (A and B) Control samples (Con) contained no added proteins. The TGFβRII-inhibiting antibody (A) and TGFβRI kinase inhibitor (B) also blocked TGFβ1-activated Smad2 signaling (***, $P < 0.0001$ in comparison with the TGFβ1 control). (C) When active endogenous TGFβ1 was blocked using 15 μg/ml of a neutralizing antibody (β1), there was a marked reduction in PF10-induced Smad2 signaling (***, $P < 0.0001$ by *t* test in comparison with the PF10 control). In the presence of anti-TGFβ1 antibody, controls with added TGFβ1 showed reduced activation of Smad2 (***, $P < 0.0001$ in comparison with the TGFβ1 control). A further control contained no added proteins. A control antibody that has no inhibitory effect on the TGFβ pathway (IgG) confirmed that the effects were caused by the specific TGFβ1 antibody. (A–C) Quantitative analysis was performed by densitometry with data normalized against β-actin. Data are represented as the mean of three repeated experiments. Error bars represent the SD of the three experiments. (D) Endogenous TGFβ1 activity produced by stimulating cells for 90 min with PF10 and PF11 at a concentration of 1 μM was assayed using the TGFβ1 EMax Immunoassay kit. The control that contained no added proteins and the fibronectin (FN) control showed no increase in active TGFβ1. (E) PF10 stimulated active and total TGFβ1 levels in cell layers and lysed cell layers. ELISA assays revealed that when 1.5 μM PF10 was incubated in fresh serum-free medium with intact cell layers (90 min), high levels of total and active TGFβ1 activation occurred with a small but statistically significant (*, $P < 0.05$ by protected *t* test) decrease in active TGFβ relative to total TGFβ. When PF10 was incubated with lysed cell layers (PF10 (L)), levels of total and active TGFβ were statistically similar, and, in both cases, 83% of levels using intact cell layers (***, $P < 0.0001$; active and total TGFβ in PF10 lysed cells compared with PF10 in unlysed cells; two-way ANOVA followed by a posthoc Tukey's test). The control that contains no added proteins and was subjected to cell lysis (Con (L)) shows a small but statistical increase in both active and total TGFβ when compared with the unlysed control (**, $P < 0.001$ by two-way ANOVA followed by a posthoc Tukey's test). Thus, PF10 releases TGFβ mainly from the cell layer. (D and E) All experiments were performed in triplicate and on the same microtitre plate (D, R^2 0.9989; E, R^2 0.9988). Error bars represent the SD of a single experiment that was undertaken in triplicate. The experiment was repeated at least three times with similar results.

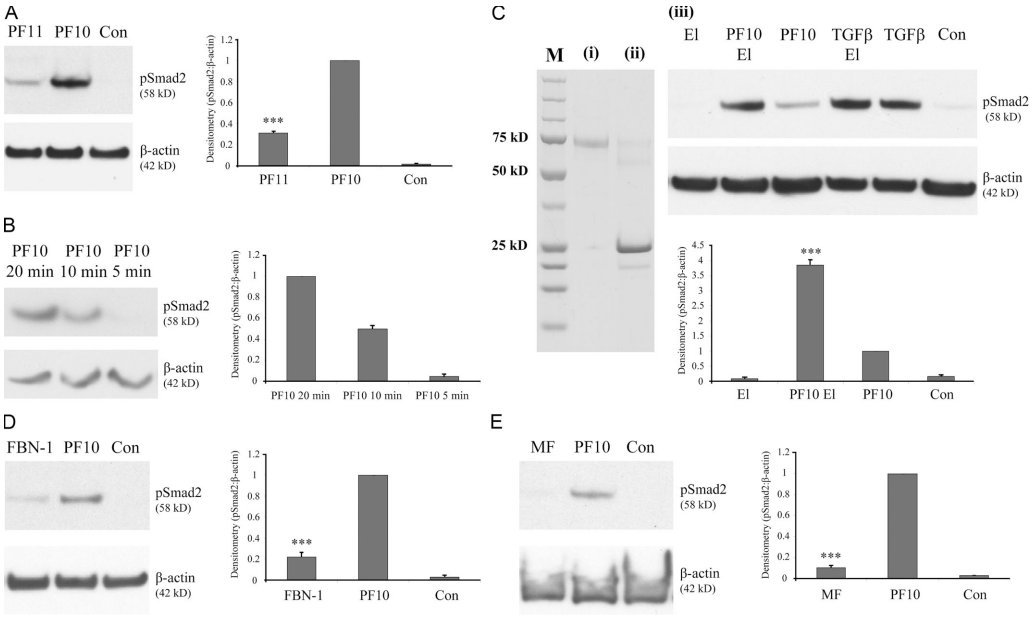

Figure 4. **Efficacies of different fibrillin-1 ligands in stimulating Smad2 phosphorylation.** (A) The ability of PF10 and PF11 to stimulate Smad2 phosphorylation was compared at equal concentrations (0.15 μM). PF10 consistently generated a stronger signal than PF11. The control well (Con) contains no added proteins. (B) Time course of PF10-induced Smad2 phosphorylation. 0.15 μM PF10 induced an increase in Smad2 phosphorylation within 10 min. (C) SDS-PAGE analysis of 0.15 μM PF10 after treatment with 0.2 mg/ml porcine pancreatic elastase, a potent protease that degrades fibrillin-1 (Kielty et al., 1994), showing the presence of degraded fragments. Lane M is a molecular marker lane; lane (i) is PF10; lane (ii) is PF10 after elastase treatment. Blots (iii) show the effects of PF10 with or without elastase treatment. After elastase, PF10 exhibited an enhanced ability to stimulate Smad2 signaling. The control, which contained no added proteins, and 0.2 mg/ml of a further elastase-only control (El) did not induce Smad2 phosphorylation. The addition of 4 nM elastase to TGFβ1 did not increase Smad2 phosphorylation. (D) 0.15 μM of purified full-length fibrillin-1 molecules (FBN-1) stimulated Smad2 phosphorylation but weakly compared with 0.15 μM PF10. The control contains no added proteins. (E) TGFβ signaling activity was barely detectable after supplementing cultures with 0.15 μM microfibrils (MF) purified from bovine ciliary zonules. 0.15 μM of the PF10 control stimulated Smad2 phosphorylation as expected. The control contains no added proteins (Con). (A–E) Quantitative analysis was performed by densitometry with data normalized against β-actin. Data are represented as the mean of three repeated experiments. Error bars represent the SD of the three experiments. ***, $P < 0.0001$ by *t* test in comparison with the PF10 control.

in the PF10-mediated stimulation of Smad2 signaling. No Smad2 signal in response to PF10 (Fig. 3 B), PF11 (not depicted), or TGFβ1 (Fig. 3 B) was detected when TGFβRI was neutralized by this inhibitor. Thus, PF10 and PF11 exert their effects on Smad2 signaling through TGFβRI and II.

Regulation of TGFβ1 by fibrillin-1 fragments and molecules

Using an antibody that specifically inhibits active TGFβ1, the Smad2 signal was markedly reduced upon stimulation with PF10 (Fig. 3 C) or PF11 (not depicted). In control experiments with supplemented TGFβ1, the inhibitory TGFβ1 antibody also blocked Smad2 phosphorylation (Fig. 3 C). Thus, Smad2 phosphorylation by PF10 or PF11 requires active TGFβ1, and fibrillin-1 does not directly activate these receptors.

Using ELISA assays, we found that the supplementation of HDF cultures with PF10 or PF11 increased active TGFβ1 in HDF serum-free medium (Fig. 3 D). After supplementing 1 μM HDF cultures for 90 min, PF10 treatment had enhanced active TGFβ1 to 23.7 pM and PF11 to 18.5 pM compared with medium from untreated HDF cultures, which contained only trace levels of TGFβ1. Positive control experiments with added recombinant active TGFβ1 contained high levels of TGFβ1 as expected. Using human plasma fibronectin, there was no increase in active TGFβ1 (R^2 0.9988; Fig. 3 D). PF10-treated cultures had slightly more total than active TGFβ1 (Fig. 3 E).

PF10, which lacks the N-terminal three domains of PF11, also consistently generated a stronger Smad2 phosphorylation signal than PF11 at equal concentrations (0.15 μM; Fig. 4 A). However, both fragments showed a similar time-dependent Smad2 signaling response in which a marked increase in phosphorylated Smad2 from 5 to 20 min was seen with PF10 (Fig. 4 B) and PF11 (not depicted).

The sequence within PF10 and PF11 that regulates active TGFβ1 levels and Smad2 signaling was localized to six cbEGF-like domains (Fig. 1, asterisk). We investigated whether its ability to enhance levels of active TGFβ was conformation dependent. After the preincubation of PF10 or PF11 with the calcium chelator EDTA at a concentration of 100 mM, increased Smad2 phosphorylation was detected in the EDTA-treated samples but not in the untreated or EDTA-only controls (unpublished data). No EDTA-induced increase in Smad2 phosphorylation was detected in control HDFs supplemented with TGFβ1 that had been preincubated with EDTA. PF10 treatment with 0.2 mg/ml elastase, which degrades PF10 (Fig. 4 C, i and ii), fibrillin molecules, and microfibrils (Kielty et al., 1994), also enhanced PF10-induced Smad2 signaling (Fig. 4 C, iii).

Full-length fibrillin-1 molecules that were purified from HDF culture medium stimulated Smad2 phosphorylation, but not as strongly as PF10 (Fig. 4 D). However, Smad2 signaling activity was barely detectable after supplementing

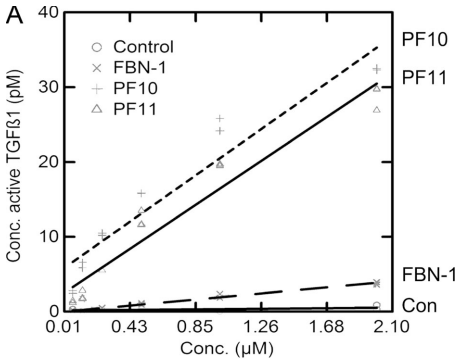

Protein	B	95% C.I.
PF10	14.777	11.610 - 17.943
PF11	14.042	11.520 - 16.564
FBN-1	1.964	1.754 - 2.174

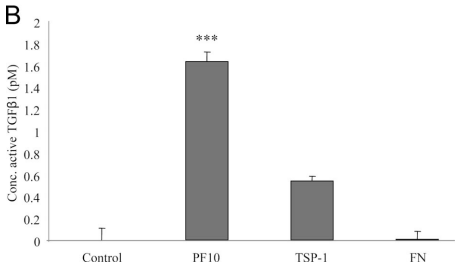

Figure 5. **Quantification of active TGFβ1 after treatment with PF10, PF11, and TSP-1.** (A) ELISA assays revealed that PF10, PF11, and fibrillin-1 molecules showed dose-dependent increases (0.0625–2 μM) in active TGFβ1 when HDF cells were stimulated for 90 min. A plot of the concentration of active TGFβ1 (picomolar) against the concentration of protein (micromolar) is shown with a regression line for each protein. The table below shows the B value and the 95% confidence interval (CI) for each protein. The slope of the regression line for PF10 is greater than that for PF11, although it is not statistically significant. PF10 shows an increase in active TGFβ1 when compared with intact fibrillin-1 molecules (R^2 0.9993). The control contained no added proteins and showed no increase in active TGFβ1. All experiments were performed in triplicate and on the same microtitre plate (R^2 0.9993). (B) Supplementation with 15 nM PF10 induced 1.1 pM more active TGFβ1 than 15 nM TSP-1 (***, $P < 0.0001$ by *t* test in comparison with TSP-1; R^2 0.9989). The control, which contained medium only, and the fibronectin (FN) control both showed no increase in active TGFβ1. All experiments were performed in triplicate and on the same microtitre plate (R^2 0.9989). Error bars represent the SD of a single experiment that was undertaken in triplicate. (A and B) The experiment was repeated at least three times with similar results.

cultures with microfibrils purified from bovine ciliary zonules (Fig. 4 E), possibly as a result of masking of the TGFβ regulatory sequence.

ELISA assays revealed that regulation of active TGFβ levels by PF10 or PF11 or by fibrillin molecules purified from HDF culture medium in the HDF cultures for 90 min was dose dependent (0.0625–2 μM). Linear regression analysis showed that the slope of the regression line for PF10 was greater than PF11, although it was not statistically significant. However, PF10 did show a statistical increase in active TGFβ1 when compared with intact fibrillin-1 molecules (R^2 0.9993; Fig. 5 A).

TSP-1 activates TGFβ1 by interacting with SLC (Young and Murphy-Ullrich, 2004). The active TGFβ1 sequence RKPK associates with the LAP sequence LSKL; SLC interactions with TSP-1 sequences KRFK and WSXW result in the release of active TGFβ1. These TSP-1 sequences are not present within PF10. A comparison of the effects of human TSP-1 and fibrillin-1

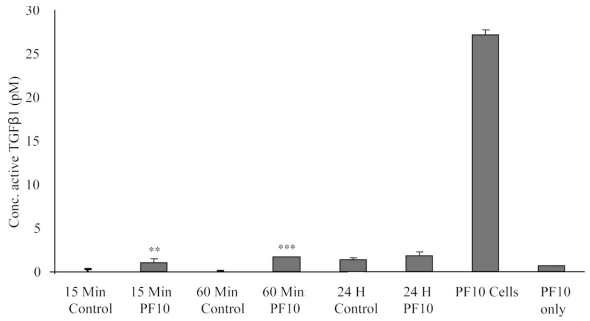

Figure 6. **PF10-mediated increase in active TGFβ1 requires cell layers.** Conditioned HDF medium that had been preincubated with HDF for 15 min, 60 min, and 24 h was stimulated with 1.5 μM PF10. In the absence of cells, PF10 induced only very low but statistically significant levels of active TGFβ1 in the 15- (**, $P < 0.001$ by *t* test) and 60-min (***, $P < 0.0001$ by *t* test) incubations compared with the controls. The conditioned medium control contains no PF10 and shows no active TGFβ1. The positive control contains 1.5 μM PF10 incubated in the presence of cells for 90 min and shows high levels of active TGFβ1. All experiments were performed in triplicate and on the same microtitre plate (R^2 0.9985). Error bars represent the SD of a single experiment that was undertaken in triplicate. The experiment was repeated at least three times with similar results.

fragment PF10 on TGFβ1 showed that at equimolar concentrations (15 nM), PF10 treatment increased 1.1 pM of active TGFβ1 more than TSP-1 (R^2 0.9989; Fig. 5 B).

Regulation of TGFβ by fibrillin-1 requires cell layers but not intact cells

Having shown that PF10 treatment increases active TGFβ1 in HDF cultures supplemented with serum-free medium, we used ELISA assays to determine whether this effect requires intact cells, cell layer ECM, or HDF-conditioned medium. 1.5 μM PF10 strongly enhanced active TGFβ1 when incubated with cell layers in freshly added serum-free medium (Fig. 6). In contrast, when PF10 was added to conditioned medium alone, it induced a very small but significant increase in active TGFβ1 at 15 and 60 min (4–7% of active TGFβ1 levels induced by cell layers; R^2 0.9985; Fig. 6).

We also compared total and active TGFβ1 levels in cell layers before and after cell lysis (Fig. 3 E). PF10 treatment of lysed cell layers led to release into serum-free medium of 83% of the levels of both total and active TGFβ1 that were released using unlysed cultures (Fig. 3 E), with no statistical difference between active and total TGFβ1 levels released from the lysed cell layers. Thus, the deposited cell layer ECM is the main requirement for the PF10-mediated increase in active TGFβ1.

Regulation of TGFβ by fibrillin-1 does not require integrin or syndecan-4 receptors

The cell lysis experiments indicated that most of the TGFβ1 regulatory effect of PF10 resided within lysed cell layers. Nevertheless, we decided to further study whether cell surface receptors influenced the PF10-mediated increase in Smad2 signaling because integrins have previously been implicated in TGFβ activation (Annes et al., 2004). The addition of integrin function–blocking antibodies to β1 or αv had no significant effect on PF10- or PF11-mediated Smad2 signaling (Fig. 7 A). The blocking antibody (mAb 16) to α5 did have a small but significant enhancing effect on TGFβ activation (Fig. 7 A); an α5-integrin–blocking antibody

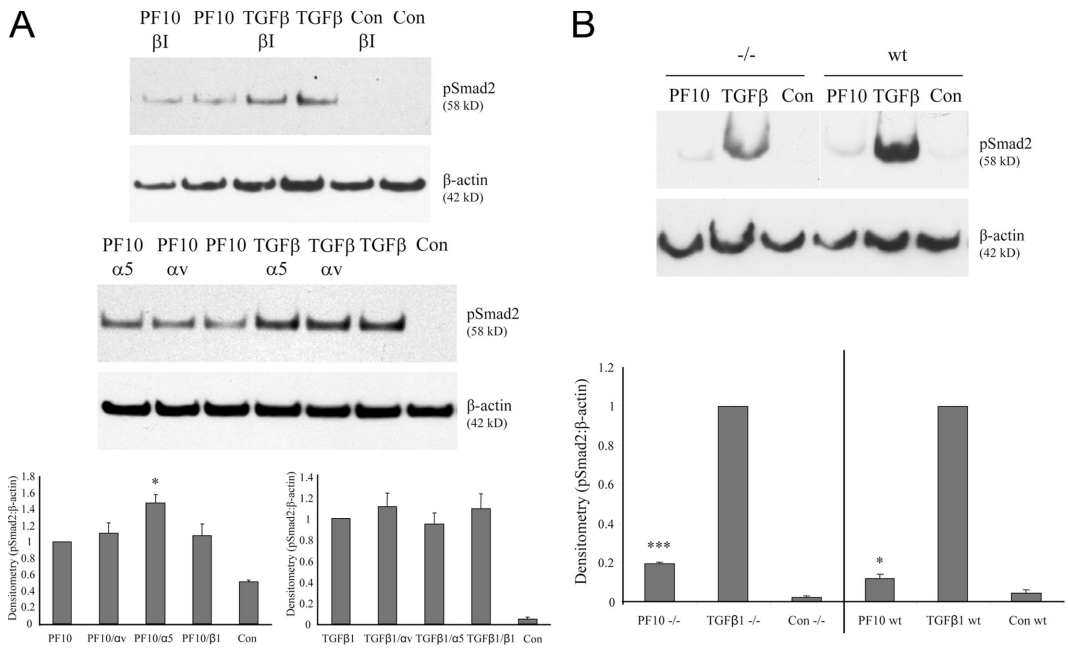

Figure 7. **Regulation of TGFβ1 by PF10 does not require cell surface receptors.** (A) 20 μg/ml of integrin function–blocking antibodies to αv (17E6) and β1 (mAb 13) had no significant inhibitory effect on the PF10-mediated stimulation of Smad2 signaling by 0.15 μM of fibrillin-1 fragment PF10. The α5-blocking antibody (mAb 16) induced a small but significant (*, $P < 0.05$ by *t* test) increase in Smad2 signaling. The control (Con), which contained no added proteins, and antibody controls (β1, αv, and α5 antibodies) showed no Smad2 phosphorylation. Active TGFβ1 was used as a positive control. (B) 0.15 μM PF10 was able to induce significant stimulation of Smad2 signaling (***, $P < 0.0001$ by *t* test in comparison with the control) in a syndecan-4–null mouse embryonic fibroblast culture, indicating that absence of the syndecan-4 receptor does not block PF10-mediated Smad2 signaling. Wild-type (wt) fibroblasts were used as a positive control (*, $P < 0.05$ by *t* test; PF10 in comparison with the control). A negative control contains no added proteins. 4 nM TGFβ1 was an additional control for Smad2 signaling. (A and B) Quantitative analysis was performed by densitometry with data normalized against β-actin. Data are represented as the mean of three repeated experiments. Error bars represent the SD of the three experiments.

has previously been shown to activate TGFβ in cultures (Matsumoto et al., 2003). However, when HDFs were coincubated with PF10 in the presence of 1.5 mM EDTA, which chelates divalent cations and inhibits integrins (Mould et al., 1995), there was no effect on the PF10-mediated increase in Smad2 signaling (unpublished data). Syndecan-4–null mouse embryonic fibroblasts significantly increased Smad2 signaling in response to PF10, as did the wild-type control fibroblasts (Fig. 7 B). Thus, PF10-mediated TGFβ regulation occurs in the absence of syndecan-4.

Regulation of TGFβ by fibrillin-1 does not involve proteolysis

Activation of TGFβ from the SLC complex can involve pericellular proteolysis (for review see Munger et al., 1997). To investigate whether proteases are involved in the fibrillin-1–mediated increase in Smad2 signaling, HDFs were preincubated for 30 min with inhibitors of serine (aprotinin and leupeptin), cysteine (leupeptin), and/or metalloproteinases (4-Abz-Gly-Pro-D-Leu-D-Ala-NH-OH). Quantitative analysis of densitometric data that was normalized against β-actin confirmed that none of these protease inhibitors had any substantial effect on PF10-stimulated Smad2 signaling (unpublished data).

Regulation of TGFβ by fibrillin-1 does not involve rapid gene expression changes in TGFβ or its receptors

PF10 and PF11 induction of TGFβ signaling could be caused by rapid changes in the gene expression of TGFβ and its receptors. mRNA samples from HDFs supplemented for 30 min with PF10 or PF11, with TGFβ1 as a positive control, or with no ligand as a negative control were used in semiquantitative RT-PCR experiments. There were no detectable differences in the expression levels of TGFβ1 and TGFβRI/II/III during the time frame of fibrillin-1–mediated enhanced TGFβ signaling (unpublished data).

Mechanism of TGFβ regulation by fibrillin-1

PF10 binds full-length fibrillin-1 in the cell layer and medium. Affinity chromatography was used to isolate secreted molecules that specifically interact with PF10 from collagenase extracts of HDF cell layers cultured in serum-free conditions. Using mass spectrometry analysis, full-length fibrillin-1 was the only ECM molecule in the insoluble cell layer that was found to bind PF10 (Table I). We detected 43 fibrillin-1 peptides, 23 of which were not present within the PF10 sequence itself. Similar results were observed when using HDF grown in medium supplemented with 10% serum. Thus, PF10 added in medium interacts specifically with fibrillin-1 in the insoluble cell layer.

PF10 binds the N-terminal region of fibrillin-1 (PF1). As we previously reported, it was not possible to coat BIAcore chips with the fibrillin-1 fragments (Cain et al., 2005; Marson et al., 2005). However, solid-phase binding assays of overlapping fibrillin-1 fragments (Fig. 1) revealed that PF10 strongly and specifically interacted with the N-terminal region of fibrillin-1 (fragment PF1) with

Table I. **Mass spectrometry of HDF cell layer proteins that bound PF10**

Protein identity	Accession no.	Mascot score	Molecular mass	No. of peptides
			D	
Fibrillin-1 precursor	P35555	1335	332,682	43
Actin, cytoplasmic 1	P60709	227	42,052	8
Tubulin β-5 chain	P05218	155	50,095	5
GAPDH	P04406	120	36,070	3

Collagenase extraction of the HDF-insoluble cell layer was undertaken with subsequent PF10 affinity chromatography. Mass spectrometry revealed that the only ECM molecule that PF10 bound in the insoluble cell layer was full-length fibrillin-1. We detected 43 fibrillin-1 peptides, 23 of which were not present within the PF10 sequence itself. The final imidazole elution contained the fibrillin-1 fragment PF10, confirming the affinity protocol (unpublished data). The identified proteins are shown in the order of Mascot score in the collagenase-extracted insoluble cell layer. The Mascot score is explained in Materials and methods. The samples were analyzed using a mass spectrometer (Micro-Q-TOF; Waters). The Mascot search engine (Matrix Science) and SwissProt database were used as previously described (Cain et al., 2006). The peptide and mass spectrometry/mass spectrometry tolerance were both ±0.3 D. GAPDH, glyceraldehyde-3-phosphate dehydrogenase. GenBank/EMBL/DDBJ accession numbers are given in the second column.

relatively high affinity (dissociation constant [K_D] = 90 ± 14 nM; Fig. 8 A). Thus, this interaction mediates the association of PF10 with full-length fibrillin-1.

We also examined the effects of two MFS disease–causing mutations in the N-terminal region (PF1) on interactions with PF10. Both MFS mutant forms of PF1 showed altered affinities for PF10. Mutant $PF1^{V449I}$ exhibited increased affinity (K_D = 52 ± 13 nM), whereas mutant $PF1^{R62C}$ bound very weakly. These altered affinities may affect PF10-stimulated Smad2 signaling and possibly MFS phenotype.

Fibrillin-1 fragments PF10 and PF1 do not bind immobilized SLC. We found no evidence for direct SLC binding to fibrillin-1 fragments PF10 or PF1 (unpublished data). Cross-linking of PF10 and SLC with bis[sulfosuccinimidyl] suberate was initially undertaken. However, no detectable band was identified that contained both PF10 and latent TGFβ1, as was previously shown for TSP-1 (Schultz-Cherry et al., 1994). A blot overlay assay with PF10 immobilized onto nitrocellulose and recombinant SLC added as a soluble ligand also failed to detect bound ligand. Furthermore, no interactions were found

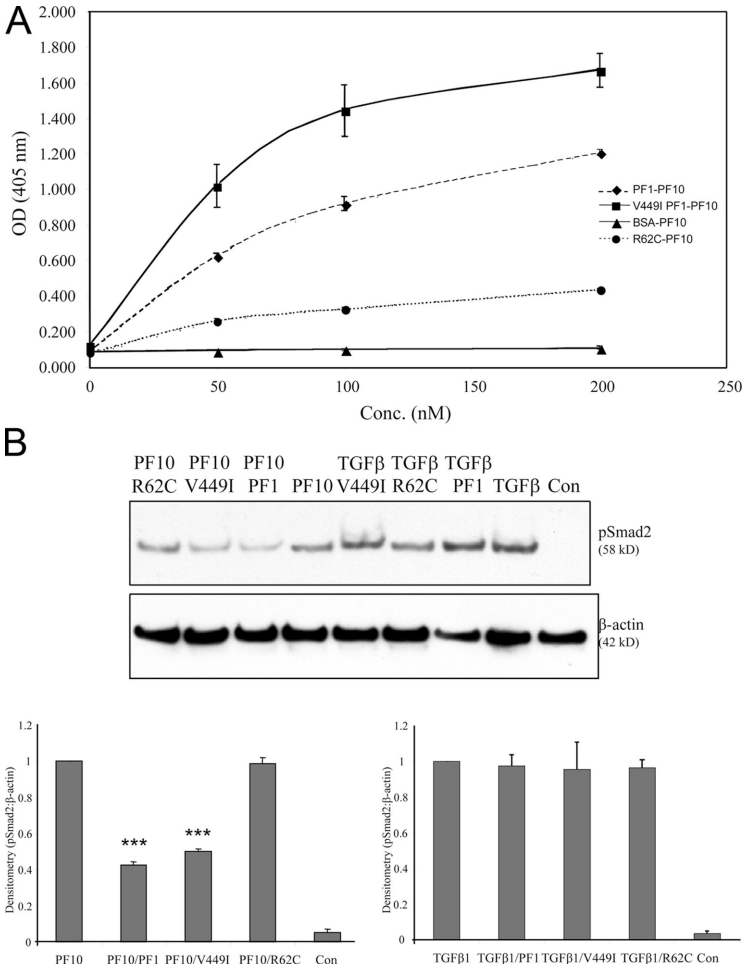

Figure 8. **PF10 interacts with the fibrillin-1 N-terminal region (PF1) and inhibits PF1 interaction with LTBP-1.** (A) Solid-phase binding assays of 0–200 nM of soluble biotinylated PF10 to 200 nM of immobilized fibrillin-1 fragments showed that PF10 interacts specifically with the N-terminal region of fibrillin-1 (PF1) with moderately strong affinity (K_D = 90 ± 14 nM). Mutant $PF1^{V449I}$ had increased affinity (K_D = 52 ± 13 nM), but mutant $PF1^{R62C}$ bound very poorly. Nonspecific binding to BSA is shown. Results are presented as the mean ± SEM (error bars) of triplicate values. (B) Preincubation of 0.15 μM PF10 and PF1 for 15 min at 20°C caused a reduction in Smad2 signaling compared with the PF10-only control (these data were normalized against corresponding β-actin; ***, $P < 0.0001$ by *t* test). Preincubation of PF10 with mutant $PF1^{V449I}$ also reduced Smad2 signaling (***, $P < 0.0001$ by *t* test in comparison with the PF10 control). However, there was no difference in Smad2 signaling after preincubation of PF10 and mutant $PF1^{R62C}$ compared with the wild-type PF10 control experiment. The negative control (Con) contains no added proteins. Quantitative analysis was performed by densitometry with data normalized against β-actin. Data are represented as the mean of three repeated experiments. Error bars represent the SD of the three experiments ($P < 0.05$ by *t* test) in comparison with the PF10 control.

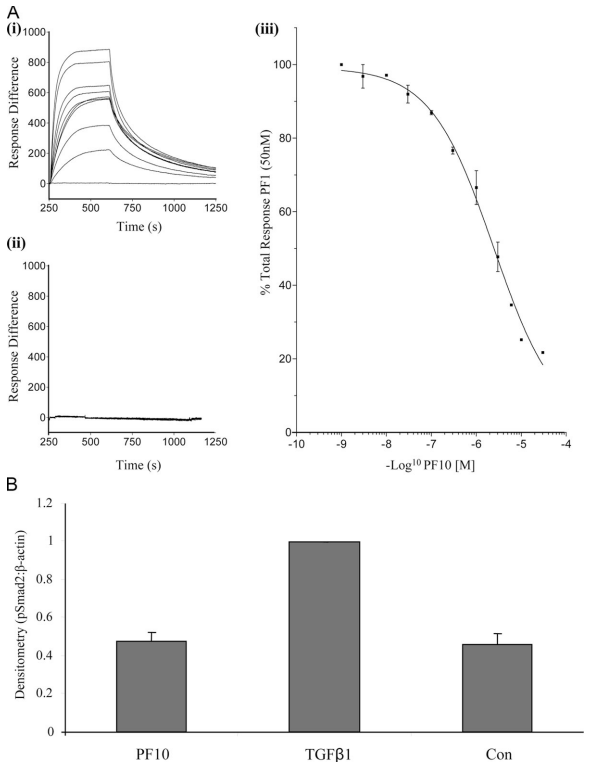

Figure 9. **PF10 inhibits the binding of PF1 and CT LTBP-1, and PF10 does not activate TGFβ1 in UMR-106 cells.** (A) BIAcore analysis of the interaction of C-terminal LTBP-1 with the fibrillin-1 N-terminal fragment PF1 as well as inhibition by PF10. Fibrillin-1 protein fragments PF1 (i) or PF10 (ii) were injected over LTBP-1 immobilized using amine coupling on a CM5 sensor chip. Both sensorgrams show analyte concentrations ranging from 0 to 150 nM, and duplicate concentrations were included in every run. One representative experiment is shown in each case. Only PF1 interacted with LTBP-1. Response difference is the difference between experimental and control flow cells in response units. Time is shown in seconds. Inhibition of the maximum response of 50 nM PF1 to LTBP-1 is shown in panel iii. Increasing concentrations of PF10 (0–30 μM) was incubated with PF1 before addition to immobilized LTBP-1. PF10 inhibited PF1 binding to LTBP-1 (IC_{50} = 2.42 ± 0.5 μM). (B) Densitometry analysis of Smad2 phosphorylation by UMR-106 cells revealed that treatment with PF10 failed to induce Smad2 signaling when compared with the control. The addition of active TGFβ1 was a positive control. No added protein was a negative control (Con). Error bars represent SD.

using BIAcore, in which fibrillin-1 fragments encompassing the entire molecule (200 nM) were passed over an SLC-immobilized chip. For these experiments, an antibody to latent TGFβ1 was used as a positive control. Recombinant MAGP-1, which binds the N-terminal fibrillin-1 fragment PF1 (Rock et al., 2004), and fibronectin also did not bind SLC.

Preincubation of PF10 with PF1 blocks PF10-stimulated Smad2 signaling. When PF10 and PF1 were preincubated for 15 min at 20°C to allow association before supplementing HDF cultures, PF10-mediated Smad2 signaling was significantly reduced compared with the PF10 control (Fig. 8 B). Mutant $PF1^{V449I}$, which binds PF10 strongly, also reduced signaling. However, there was no difference in Smad2 signaling of mutant $PF1^{R62C}$, which binds PF10 weakly, compared with the PF10 control. These experiments show that the PF10–PF1 interaction is directly involved in increasing Smad2 signaling.

Preincubation of PF10 with PF1 inhibits the binding of LTBP-1 to PF1. An N-terminal fibrillin-1 interaction with the C-terminal region of LTBP-1 has been predicted to stabilize LLC on microfibrils (Isogai et al., 2003; for review see Ramirez et al., 2004). Using BIAcore analysis, we first confirmed this N-terminal fibrillin-1 (PF1) interaction with the C-terminal region of LTBP-1 (Fig. 9 A, i). The K_D for this PF1–LTBP-1 interaction was 43.1 ± 5.9 nM. Subsequent BIAcore experiments confirmed that PF10 did not bind LTBP-1 (Fig. 9 A, ii) and revealed that preincubation of PF1 with increasing concentrations of PF10 specifically inhibited the PF1–LTBP-1 interaction (Fig. 9 A, iii). The IC_{50} for this PF10 inhibition was 2.42 ± 0.5 μM. Thus, PF10 can regulate TGFβ1 bioavailability by displacing LTBP-1 from fibrillin-1 and displacing LLC from microfibrils.

PF10 fails to stimulate Smad2 signaling in the absence of microfibrils. Using the rat UMR-106 cell line that does not constitutively express or deposit fibrillin-1 or LTBP-1 (Dallas et al., 2000), PF10 had no significant effect on Smad2 signaling (Fig. 9 B). This result supports the requirement for fibrillin microfibrils and LTBP-1 in PF10-stimulated Smad2 signaling.

Discussion

Recent studies have shown that a major functional relationship exists between fibrillin-1 and TGFβ activity (for reviews see Ramirez et al., 2004; Dietz et al., 2005). Fibrillin-1 is postulated to regulate TGFβ through the association of LLC with fibrillin-rich microfibrils, although it is not clear how this regulation occurs. We have discovered that a specific fibrillin-1 sequence encoded by exons 44–49 (in recombinant fragments PF10 and PF11) enhances endogenous active TGFβ1 and Smad2 signaling. This sequence, which is present within a pepsin-resistant microfibril proteolytic fragment (Maslen et al., 1991), contains no TB motif such as those in LTBP-1 and -3 that bind LAP through disulphide linkage (for review see Hyytiäinen et al., 2004). Thus, fibrillin-1 enhances active TGFβ1 by a novel mechanism and may contribute directly to the lung, skeletal, and vascular pathologies of MFS and related diseases.

We excluded the idea that purified PF10 or PF11 contained traces of latent or active TGFβ by mass spectrometry and immunoblotting, and we did not detect any TGFβ1 activity in our purified PF10 or PF11 preparations. The smaller fibrillin-1 sequences tested had greater ability to stimulate Smad2 signaling. PF10 induced slightly greater levels of active TGFβ and Smad2 signaling than PF11, which comprises PF10 plus three additional upstream domains, and both fragments induced greater levels of active TGFβ and Smad2 signaling than intact fibrillin. Small-angle x-ray analysis and single-particle transmission electron microscopy of the solution structure of fibrillin-1 recently revealed that the region spanning TB4 to TB6 (PF11) is relatively compact, with PF10 being the most linear region within PF11 (Baldock et al., 2006). The additional three-domain globular region of PF11 and other domains in full-length fibrillin-1 may exert conformational effects that reduce the availability of the sequence encoded by exons 44–49. We previously showed

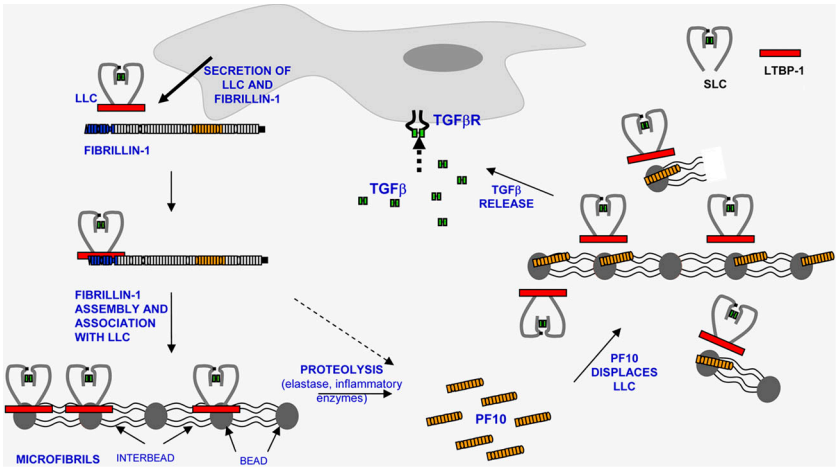

Figure 10. **Model of how PF10 regulates TGFβ bioavailability.** Secreted LLC becomes associated with deposited fibrillin microfibrils (LTBP-1, a component of LLC, is shown in red). The PF10 fragment (orange), which is released by proteolysis, binds microfibrillar fibrillin-1 within the insoluble cell layer, interacting specifically with the fibrillin-1 N-terminal region (PF1; blue). PF10 binds assembled microfibrils at or adjacent to the beads where this N-terminal region localizes (Reinhardt et al., 1996; Baldock et al., 2001). PF10 inhibits the PF1 interaction with LTBP-1 (and thus with LLC), leading to the release of LLC and an increase in active TGFβ. Microfibril beads (gray ovals) and interbead regions (lines between ovals) are indicated.

that elastase effectively degrades microfibrils and fibrillin molecules (Kielty et al., 1994), and, here, we have found that the elastase degradation of PF10 enhances Smad2 signaling. In tissues, such proteolytic fragments may potently stimulate TGFβ-induced signaling. We found only trace levels of Smad2 signaling induced by tissue-purified microfibrils. The active PF10 sequence may be masked by molecular folding and/or by associated molecules. We previously mapped this fibrillin-1 region to the microfibril interbead (Baldock et al., 2001).

TSP-1 has previously been identified as a physiological activator of TGFβ (Schultz-Cherry et al., 1994). ELISA dose-response curves have revealed that PF10 was more effective at activating endogenous TGFβ1 than TSP-1. The active TGFβ sequence RKPK associates with the LAP sequence LSKL in the SLC (Young and Murphy-Ullrich, 2004); the TSP-1 activation of TGFβ involves competitive binding of a TSP-1 sequence (KRFK) that releases TGFβ from SLC. Sequence analysis of the six cbEGF domains in PF10 that regulate TGFβ bioavailability revealed no similar motifs, so PF10-mediated TGFβ1 activation involves a different mechanism.

Latent TGFβ can also be activated by integrin αvβ6 or proteolysis (Annes et al., 2004; Fontana et al., 2005). However, PF10-mediated regulation of TGFβ1 did not involve cell surface β1- or αv-integrin receptors, syndecan-4, or pericellular proteolysis. Moreover, changes in TGFβ-induced signaling could not be accounted for by the enhanced expression of TGFβ or its receptors.

To determine how fibrillin-1 enhances active TGFβ and stimulates Smad2 signaling, we first investigated what PF10 interacts with in HDF cultures. Mass spectrometry revealed that PF10 bound specifically to full-length fibrillin-1 in the microfibril-rich insoluble fibroblast layer, which is a proposed repository of LLC (for review see Ramirez et al., 2004), and also bound with high affinity to the N-terminal fibrillin-1 fragment PF1 in solid-phase binding assays. The PF1 sequence localizes adjacent to microfibril beads (Reinhardt et al., 1996; Baldock et al., 2001). We found no evidence for SLC interactions with either PF10 or PF1 or for LTBPs interacting directly with PF10. Crucially, however, preformed PF10–PF1 complexes reduced PF10-induced Smad2 signaling, confirming a key role for this interaction in regulating active TGFβ1. Moreover, MFS mutant PF1 fragments that had increased or decreased affinity for PF10 showed reduced or unchanged Smad2 signaling, respectively. Next, we showed that the PF10 interaction with PF1 directly inhibits C-terminal LTBP-1 binding to the fibrillin-1 N terminus so that, at appropriate concentrations, it will displace LLC from microfibrils. Finally, we confirmed that PF10 has no effect on Smad2 signaling in UMR-106 cell cultures, which do not constitutively express fibrillin-1 or LTBP-1 (Dallas et al., 2000). Thus, we have delineated a novel mechanism that regulates TGFβ bioavailability (Fig. 10) in which PF10, by binding microfibrils close to the beads through interactions with the fibrillin-1 N-terminal sequence, can displace LTBP-1 and LLC from microfibrils. One possible mechanism of subsequent TGFβ activation may be the BMP-1 cleavage of LTBP-1 (Ge and Greenspan, 2006). Alternatively, TGFβ may become activated during the release of LLC from microfibrils through conformational changes because fibrillin-1– and SLC-binding sites are within the same C-terminal region of LTBP-1. The LTBP-1 N terminus can be transglutaminase linked to ECM (for review see Rifkin, 2005), but release of the LTBP-1 C terminus from microfibrils may be sufficient for TGFβ activation.

Further experiments confirmed that PF10 releases TGFβ1 mainly from lysed cell layers as expected because fibrillin-1 is a major deposited ECM component. The small increase in TGFβ1 levels when cells are intact may be caused by additional microfibrils assembling at the cell surface. Low levels of active TGFβ1 released by PF10 from conditioned medium probably reflect the known presence of some secreted fibrillin-1 molecules and aggregates in medium (Reinhardt et al., 2000a; unpublished data).

Enhanced PF10-mediated Smad2 signaling after EDTA treatment indicates that calcium-dependent conformation of the cbEGF-like domain array influences activation, perhaps by altering the PF1–PF10 interaction. We have also found that supplementing cultures with heparin enhances PF10-dependent TGFβ activation, but we have excluded that this heparin effect is caused by direct heparin–PF10 interactions (unpublished data). Heparin strongly binds PF1 in a conformation-dependent

manner (Cain et al., 2005; unpublished data), so we speculate that it may enhance LTBP-1 displacement from PF1 by PF10.

Pathological fibrillin-1–mediated regulation of TGFβ bioavailability may be induced by microfibril degradation products. Progressive proteolytic damage and aortic degeneration are hallmarks of classic MFS. Disease-causing amino acid substitutions are spread throughout the molecule (for review see Robinson et al., 2006), but some mutations occur within PF10 that may directly alter TGFβ activation. They include classic MFS causing amino acid substitutions in exons 44 and 46, exon 47/48 domain interface, exons 47 and 48, and deletions of exons 44, 44–46, 46, and 49 (www.umd.be). Furthermore, mutations in any region of fibrillin-1 that disrupt domain and molecular conformations can increase proteolytic susceptibility to inflammatory enzymes (Ashworth et al., 1999; Booms et al., 2000; Reinhardt et al., 2000b; Suk et al., 2004; Vollbrandt et al., 2004), leading to microfibril proteolysis and release of TGFβ-regulating fragments. Microfibrils from unaffected individuals are also highly susceptible to degradation by matrix proteases such as elastase (Ashworth et al., 1999). Thus, microfibril proteolysis could be a common mechanism for the release of active TGFβ1 from ECM in heritable and acquired fibrillinopathies. In summary, we have shown that a specific fibrillin-1 sequence regulates the bioavailability of TGFβ1. We are currently investigating whether fibrillin-1 similarly regulates levels of other TGFβ isoforms and whether other fibrillins can regulate TGFβ.

Materials and methods

Cell cultures

Tissue culture reagents were purchased from Life Technologies or Mediatech. 293-EBNA cells were purchased from the American Type Tissue Culture Collection and were routinely maintained in DME with 10% FBS, 2 mM L-glutamine, 100 U/ml penicillin/streptomycin, and 250 μg/ml G418. HDFs were purchased from Cascade Biologics, Inc. and maintained in low serum growth supplement from the same supplier. UMR-106 rat osteosarcoma cells were originally obtained from T.J. Martin (St Vincent Institute of Medical Research, Fitzroy, Victoria, Australia). 2T3 cells were a gift from S. Harris (University of Texas Health Science Center, San Antonio, TX; Ghosh-Choudhury et al., 1996).

Expression and purification of recombinant fibrillin-1

Recombinant fibrillin-1 fragments encompassing full-length human fibrillin-1 were expressed in 293-EBNA cells using a modified pCEP-His vector and were purified as previously described (Fig. 1; Cain et al., 2005; Marson et al., 2005). Secreted fibrillin molecules and multimers were purified from confluent HDF culture medium by cesium chloride density gradient centrifugation and size fractionation using a Sephacryl 200 column equilibrated in 0.1 M NaCl, 1 mM $CaCl_2$, and 50 mM Tris, pH 8.0. Identity and purity were confirmed by immunoblotting using an anti–fibrillin-1 mAb raised to the N terminus (amino acids 45–450; mAb 2502; Chemicon Europe) and by mass spectrometry (provided by B. Raynal, University of Manchester, Manchester, UK). Microfibrils were purified from adult bovine ciliary zonules as previously described (Kielty et al., 1998). The presence of microfibrils was confirmed using atomic force microscopy (Sherratt et al., 2004).

Expression and purification of recombinant C-terminal LTBP-1

A C-terminal fragment of human LTBP-1 (amino acids 1,008–1,394) was generated by PCR amplification using Vent DNA polymerase (New England Biolabs, Inc.), a high fidelity DNA polymerase, according to the manufacturer's instructions. The template was human LTBP-1 cDNA in the vector pSV7d (a gift from K. Miyazono, University of Tokyo, Tokyo, Japan). A 10-histidine epitope tag was engineered into the primers at the C terminus of the recombinant LTBP-1 fragments. The PCR products were ligated into pCEP-Pu expression vector (a gift from E. Kohfeldt, Max Planck Institute of Biochemistry, Martinsried, Germany) in frame with the BM40 signal sequence. Insert sequences were confirmed by automated sequencing (MWG). Constructs were transfected into 293-BNA cells using LipofectAMINE 2000 (Invitrogen). Transfected cells were selected in 1 μg/ml puromycin, and resistant cells were expanded into triple-layer flasks. Recombinant fragments were purified using a nickel-NTA agarose column (QIAGEN) according to the manufacturer's instructions. Bound protein was eluted with low pH or with 100–300 mM imidazole. The protein was further purified using a mono-Q ion exchange column in conjunction with a protein purification system (BioCad 700E; Applied Biosystems). Bound protein was eluted with a linear 0–1-M NaCl gradient. Coomassie blue staining was used to visualize the purity of the fragment, and mass spectrometry/peptide mass mapping was used to validate the recombinant LTBP-1 fragment.

Smad2 signaling assays

Confluent HDFs were incubated for 24 h using serum-free DME supplemented with 4.5 g/L glucose and L-glutamine (Cascade Biologics, Inc.). The cells were incubated in 0.5 ml of fresh serum-free DME containing 0.15 μM of recombinant fibrillin-1 fragments, 0.15 μM of medium-purified fibrillin-1 molecules, or 0.15 μM of tissue-purified microfibrils for 15 min at 37°C. 4 nM of recombinant human TGFβ1 (Sigma-Aldrich) was used as a positive control. Human plasma fibronectin was used as an additional control (FC010; Chemicon Europe). Cells were washed twice with PBS, incubated with NET buffer supplemented with fresh proteinase inhibitors (20 mM Tris-HCl, pH 8.0, 150 mM NaCl, 1% NP-40, 2.5 mM EDTA, 100 μM Na_3VO_4, 1% aprotinin, 1 mM PMSF, and 1% leupeptin) for 30 min, and scraped from the tissue culture flask. Cell lysates were electrophoresed, and Western blots were undertaken using a Smad 2 antibody (AB3849; Chemicon Europe). Western blots were developed using electrochemiluminescence (GE Healthcare). M_r film (BioMax; Kodak) was used to visualize positive bands. Each Western blot was stripped after use and reprobed with β-actin to ensure equal loadings of total protein (AC-15; Sigma-Aldrich). In some experiments, the effects of pretreating fibrillin-1 fragments with EDTA, elastase, or heparin were determined. Protein fragments were preincubated with 100 mM EDTA, pH 7.4, 100 μg/ml heparin (3,000 kD; Sigma-Aldrich), or 0.2 mg/ml porcine pancreatic elastase (Sigma-Aldrich) for 15 min before SDS-PAGE and Western blot analysis of Smad2 signaling. Signaling assays were also performed using the mouse osteoblast cell line 2T3 (Ghosh-Choudhury et al., 1996), syndecan-4–null and wild-type mouse embryonic fibroblast cell lines (gift from M.J. Humphries, University of Manchester, Manchester, UK), and UMR-106 rat osteosarcoma cells (gift from T.J. Martin). Quantitative analysis was performed by densitometry with data normalized against β-actin. The densitometry values are plotted as a ratio of Smad2 signaling against corresponding β-actin. Data are represented as the mean of three repeated experiments and were statistically analyzed using unpaired *t* tests (Prism 2.0 software; GraphPad). Error bars represent the SD of the three experiments. Results are statistically significant when the p-value is <0.05 (*, $P < 0.05$; **, $P < 0.001$; ***, $P < 0.0001$).

Smad2 signaling inhibition assays

HDFs were incubated with inhibitory antibodies or chemical inhibitors for 30 min at 37°C in 0.5 ml of serum-free DME before lysis and signaling assays (as described in the previous section). An anti-TGFβ1 mAb (mAb 240; R&D Systems) and an anti–human TGFβRII antibody (AF-241-NA; R&D Systems), which was designated RII in Fig. 3 A, were used at concentrations of 15 μg/ml. A chemical inhibitor of TGFβRI, [3-(pyridin-2-yl)-4-(4-quinonyl)]-1H-pyrazole (Merck Biosciences), which is designated as RI in Fig. 3 B, was used at a concentration of 20 μg/ml. The inhibitory integrin antibodies αv (17E6; Merck Biosciences), α5 (mAb 16), and β1 (mAb 13; gifts from M.J. Humphries) were used at concentrations of 20 μg/ml. Freshly prepared protease inhibitors were used at neutral pH at the following concentrations: aprotinin (serine) at 100 μM, leupeptin (cysteine; Sigma-Aldrich) at 100 μM, and a matrix metalloproteinase inhibitor (4-Abz-Gly-Pro-D-Leu-D-Ala-NH-OH; inhibits matrix metalloproteinases 1, 3, 8, and 9; Merck Biosciences) at 150 μM. Quantitative analysis was performed by densitometry with data normalized against β-actin. The densitometry values are plotted as a ratio of Smad2 signaling against corresponding β-actin.

ELISA assays for active and total TGFβ1

The amounts of active TGFβ1 present in HDF medium were determined using the TGFβ1 EMax Immunoassay kit (Promega). Recombinant fragments were added to HDFs in 0.5 ml of serum-free DME for 90 min at

37°C. The media were collected, and 200 µl was used in the EMax immunoassay, which was performed according to the manufacturer's instructions. For measurement of total (active + latent) TGF, the samples were acidified using HCl and were reneutralized before measurement using NaOH according to the ELISA manufacturer's instructions (Promega; Dallas et al., 2005). TGFβ standard curves were undertaken for every assay. The standard curve is linear between 15.6 and 1,000 pg/ml of the TGFβ1 standard. All experiments were performed in triplicate and on the same microtitre plate. The data are represented as the mean values of one experiment. In some cases, other statistical methods were used: linear regression analysis was undertaken using SPSS 12.0 software (SPSS), and two-way analysis of variance (ANOVA) was performed followed by a posthoc multiple comparisons test using Tukey's test (SPSS 12.0 software). Furthermore, a protected two-tailed *t* test was performed in conjunction with ANOVA in some cases.

Semiquantitative RT-PCR

Recombinant proteins were added to HDFs in 0.5 ml of serum-free DME for 90 min at 37°C. Total RNA was isolated using the SV Total RNA Isolation kit (Promega). RNA was quantitated using an RNA/DNA calculator (GeneQuant Pro; GE Healthcare). cDNA was synthesized from the extracted RNA using RT-PCR, and the products were resolved using 2.5% ultrapure agarose gels (Invitrogen). Oligonucleotide primers for PCR were designed using Primer3 software.

Affinity chromatography and mass spectrometry

0.5 mg of the fibrillin-1 fragment PF10 was bound to a nickel chelate affinity chromatography column using a chromatography system (AKTAprime; GE Healthcare). HDF cell layers that had been lysed with NET buffer containing fresh protease inhibitors (20 mM Tris-HCl, pH 8.0, 150 mM NaCl, 1% NP-40, 2.5 mM EDTA, 100 µM Na_3VO_4, 1% aprotinin, 1 mM PMSF, and 1% leupeptin) were passed over the column followed by a wash using 150 mM NaCl, 50 mM Tris-HCl, and 1 mM $CaCl_2$, pH 7.4. The bound proteins were subsequently eluted using a gradient of 1 M NaCl, 50 mM Tris-HCl, and 1 mM $CaCl_2$, pH 7.4. The procedure was repeated using the insoluble cell layer after treatment with 0.5 mg/ml collagenase in the presence of protease inhibitors (2 mM PMSF and 5 mM *N*-ethylmaleimide) in 150 mM NaCl, 50 mM Tris-HCl, and 1 mM $CaCl_2$, pH 7.4, for 24 h. After eluting bound molecules, the affinity column was subjected to a final elution step using 500 mM imidazole, 150 mM NaCl, 50 mM Tris-HCl, pH 7.4, and 0.5 mM $CaCl_2$. All fractions were desalted using a HiTrap desalting column (GE Healthcare). All samples were reduced and alkylated as previously described (Cain et al., 2006). To identify proteins bound to PF10, samples were analyzed using a mass spectrometer (Micro-Q-TOF; Waters) and the Mascot search engine (Matrix Science). The Mascot protein score is derived from the sum of the ion scores for each peptide detected from that protein. The ion score of a peptide, which reflects the probability of the observed peptide mass matching the mass of the peptide in the database, is expressed as a value, $\log_{10}(P)$, where P is the probability (Perkins et al., 1999). The SwissProt database was used. Peptide tolerance and mass spectrometry/mass spectrometry tolerance were set to ±0.3 D. In the final imidazole elution, PF10 was the only ECM sequence, which confirmed the affinity protocol.

Solid-phase binding

Solid-phase binding was performed as previously described (Marson et al., 2005). In brief, 0–200 nM of soluble ligands were biotinylated, and flat-bottomed microtitre plates (Thermo Labsystems) were coated with the N-terminal fibrillin-1 fragment (PF1) at 200 nM in TBS (50 mM Tris-HCl, pH 7.4, and 0.1 M NaCl) overnight at 4°C. BSA blocking, washing, binding, and detection steps were subsequently performed. Soluble biotinylated protein dilutions of 0–200 nM for binding curves were used. All assays were performed in triplicate and were repeated at least twice to confirm the observed results. K_D values for dose-dependent interactions were calculated using nonlinear regression with one-site binding (hyperbola). All data are shown as mean values ± SEM.

Chemical cross-linking

1 µg of the fibrillin-1 fragment PF10 was incubated with 1 µg of recombinant latent TGFβ1 for 2 h at 37°C. The cross-linking agent BS^3 (bis[sulfosuccinimidyl] suberate; Pierce Chemical Co.) was added at a concentration of 0.25 mM and incubated for 15 min at 4°C. The proteins were electrophoresed, and potential bands of interest were analyzed using mass spectrometry as outlined above (see Affinity chromatography and mass spectrometry).

Blot overlay assay

Blot overlays were performed essentially as previously described (Isogai et al., 2003). 25 µg of the fibrillin-1 fragment PF10 was electrophoresed using SDS-PAGE and was transferred onto nitrocellulose as described in the Smad2 signaling assays section. The membranes were blocked and incubated with 50 µg/ml of latent TGFβ1 (299-LT/CF; R&D Systems) at 4°C overnight. A primary antibody to latent TGFβ1 (AF-246-NA; R&D Systems) followed by an enzyme-conjugated secondary antibody was used to detect bound ligand. Blots were developed using enhanced chemiluminescence as described in the Smad2 signaling assays section.

BIAcore 3000 analysis

Kinetic binding analysis of latent TGFβ1 with fibrillin-1 was undertaken by surface plasmon resonance using a biosensor (BIAcore 3000; BIAcore). To investigate possible interactions between fibrillin-1 and the SLC, 1.8 µg/ml of latent TGFβ1 (299-LT/CF; R&D Systems) was immobilized onto a CM5 sensor chip in 10 mM acetic acid, pH 5.5. All subsequent binding experiments were performed in 10 mM Hepes, pH 7.4, 0.1 M NaCl, 1 mM $CaCl_2$, and 0.005% surfactant P20. 200 nM of fibrillin-1 fragments were applied to the sensor chip at a flow rate of 30 µl/min for 3 min. After 2.5-min dissociation, the chip was regenerated using 50 mM acetic acid for 30 s. The response value for each injection was calculated using the binding assay result wizard (BIAcore control software 3.2; BIAcore). As a positive control, an SLC antibody (AF-246-NA; R&D Systems) was passed over the chip.

To analyze the binding of fibrillin-1 fragments to LTBP-1, a C-terminal fragment of LTBP-1 (designated CT LTBP-1; residues 1,008–1,394) was immobilized onto a CM5 sensor chip at 25 µg/ml in 50 mM sodium acetate, pH 5.2. 0–150 nM of the fibrillin-1 fragments PF1 and PF10 were applied to the sensor chip (15 µl/min) for 6 min and were left to dissociate for 10 min. Regeneration was performed in 10 mM Hepes, pH 7.4, 0.4 M NaCl, 1 mM $CaCl_2$, and 0.005% surfactant P20. The K_D for the PF1 interaction was calculated by plotting a saturation binding curve using the equilibrium response value at the top of the curve as described previously (Cain et al., 2005). The PF1 interaction was performed three times, and the final K_D was calculated from a mean of these values.

Increasing concentrations of PF10 (0–30 µM) were preincubated with 50 nM PF1 for 15 min before being applied to the sensor chip for 3 min (30 µl/min) and were left to dissociate for 10 min. CT LTBP-1 on the sensor surface was then regenerated. The maximum response was plotted against concentration using Prism 2.0 software (GraphPad). No binding response occurred between PF10 and CT LTBP-1, so it was possible to determine whether PF10 inhibits the interaction between PF1 and CT LTBP-1. The IC_{50} was calculated using nonlinear regression analysis (sigmoidal dose response; variable slope).

We thank Dr. B. Raynal for purified fibrillin-1 molecules and Prof. M.J. Humphries for syndecan-4–null and wild-type mouse embryonic fibroblast cell lines and integrin antibodies. We also thank Dr. R. Preziosi for statistical analysis support.

This work was funded by the UK Medical Research Council (MRC), the UK Centre for Tissue Engineering (MRC, Biotechnology and Biological Sciences Research Council, and Engineering and Physical Sciences Research Council), and the British Heart Foundation. C.M. Kielty is a Royal Society-Wolfson Research Merit Award holder.

Submitted: 30 August 2006
Accepted: 20 December 2006

References

Ades, L.C., K. Sullivan, A. Biggin, E.A. Haan, M. Brett, K.J. Holman, J. Dixon, S. Robertson, A.D. Holmes, J. Rogers, and B. Bennetts. 2006. FBN1, TGFBR1, and the Marfan-craniosynostosis/mental retardation disorders revisited. *Am. J. Med. Genet. A.* 140:1047–1058.

Annes, J.P., J.S. Munger, and D.B. Rifkin. 2003. Making sense of latent TGFβ activation. *J. Cell Sci.* 116:217–224.

Annes, J.P., Y. Chen, J.S. Munger, and D.B. Rifkin. 2004. Integrin $\alpha_v\beta_6$-mediated activation of latent TGF-β requires the latent TGF-β binding protein-1. *J. Cell Biol.* 165:723–734.

Ashworth, J.L., G. Murphy, M.J. Rock, M.J. Sherratt, S.D. Shapiro, C.A. Shuttleworth, and C.M. Kielty. 1999. Fibrillin degradation by matrix metalloproteinases: implications for connective tissue remodelling. *Biochem. J.* 340:171–181.

Baldock, C., A.J. Koster, U. Ziese, M.J. Rock, M.J. Sherratt, K.E. Kadler, C.A. Shuttleworth, and C.M. Kielty. 2001. The supramolecular organization of fibrillin-rich microfibrils. *J. Cell Biol.* 152:1045–1056.

Baldock, C., V. Siegler, D.V. Bax, S.A. Cain, K.T. Mellody, A. Marson, J.L. Haston, R. Berry, M.C. Wang, J.G. Grossmann, et al. 2006. Nanostructure of fibrillin-1 reveals compact conformation of EGF arrays and mechanism for extensibility. *Proc. Natl. Acad. Sci. USA*. 103:11922–11927.

Booms, P., F. Tiecke, T. Rosenberg, C. Hagemeier, and P.N. Robinson. 2000. Differential effect of FBN1 mutations on in vitro proteolysis of recombinant fibrillin-1 fragments. *Hum. Genet.* 107:216–224.

Cain, S.A., C. Baldock, J. Gallagher, A. Morgan, D.V. Bax, A.S. Weiss, C.A. Shuttleworth, and C.M. Kielty. 2005. Fibrillin-1 interactions with heparin. Implications for microfibril and elastic fiber assembly. *J. Biol. Chem.* 280:30526–30537.

Cain, S.A., A. Morgan, M.J. Sherratt, S.G. Ball, C.A. Shuttleworth, and C.M. Kielty. 2006. Proteomic analysis of fibrillin-rich microfibrils. *Proteomics*. 6:111–122.

Dallas, S.L., D.R. Keene, S.P. Bruder, J. Saharinen, L.Y. Sakai, G.R. Mundy, and L.F. Bonewald. 2000. Role of the latent transforming growth factor beta binding protein 1 in fibrillin-containing microfibrils in bone cells in vitro and in vivo. *J. Bone Miner. Res.* 15:68–81.

Dallas, S.L., P. Sivakumar, C.J. Jones, Q. Chen, D.M. Peters, D.F. Mosher, M.J. Humphries, and C.M. Kielty. 2005. Fibronectin regulates latent transforming growth factor-beta (TGF beta) by controlling matrix assembly of latent TGF beta-binding protein-1. *J. Biol. Chem.* 280:18871–18880.

Dietz, H.C., B. Loeys, L. Carta, and F. Ramirez. 2005. Recent progress towards a molecular understanding of Marfan syndrome. *Am. J. Med. Genet. C. Semin. Med. Genet.* 139:4–9.

Feng, X.H., and R. Derynck. 2005. Specificity and versatility in TGF-beta signaling through Smads. *Annu. Rev. Cell Dev. Biol.* 21:659–693.

Fontana, L., Y. Chen, P. Prijatelj, T. Sakai, R. Fassler, L.Y. Sakai, and D.B. Rifkin. 2005. Fibronectin is required for integrin $\alpha_v\beta_6$-mediated activation of latent TGF-beta complexes containing LTBP-1. *FASEB J.* 19:1798–1808.

Ge, G., and D.S. Greenspan. 2006. BMP1 controls TGFβ1 activation via cleavage of latent TGFβ-binding protein. *J. Cell Biol.* 175:111–120.

Ghosh-Choudhury, N., J.J. Windle, B.A. Koop, M.A. Harris, D.L. Guerrero, J.M. Wozney, G.R. Mundy, and S.E. Harris. 1996. Immortalized murine osteoblasts derived from BMP-2-T-antigen expressing transgenic mice. *Endocrinology*. 137:331–339.

Gomez-Duran, A., S. Mulero-Navarro, X. Chang, and P.M. Fernandez-Salguero. 2006. LTBP-1 blockade in dioxin receptor-null mouse embryo fibroblasts decreases TGF-beta activity: Role of extracellular proteases plasmin and elastase. *J. Cell. Biochem.* 97:380–392.

Gregory, K.E., R.N. Ono, N.L. Charbonneau, C.L. Kuo, D.R. Keene, H.P. Bachinger, and L.Y. Sakai. 2005. The prodomain of BMP-7 targets the BMP-7 complex to the extracellular matrix. *J. Biol. Chem.* 280:27970–27980.

Habashi, J.P., D.P. Judge, T.M. Holm, R.D. Cohn, B.L. Loeys, T.K. Cooper, L. Myers, E.C. Klein, G. Liu, C. Calvi, et al. 2006. Losartan, an AT1 antagonist, prevents aortic aneurysm in a mouse model of Marfan syndrome. *Science*. 312:117–121.

Hyytiäinen, M., C. Penttinen, and J. Keski-Oja. 2004. Latent TGF-beta binding proteins: extracellular matrix association and roles in TGF-beta activation. *Crit. Rev. Clin. Lab. Sci.* 41:233–264.

Isogai, Z., R.N. Ono, S. Ushiro, D.R. Keene, Y. Chen, R. Mazzieri, N.L. Charbonneau, D.P. Reinhardt, D.B. Rifkin, and L.Y. Sakai. 2003. Latent transforming growth factor beta-binding protein 1 interacts with fibrillin and is a microfibril-associated protein. *J. Biol. Chem.* 278:2750–2757.

Kielty, C.M. 2006. Elastic fibres in health and disease. *Expert Rev. Mol. Med.* 8:1–23.

Kielty, C.M., D.E. Woolley, S.P. Whittaker, and C.A. Shuttleworth. 1994. Catabolism of intact fibrillin microfibrils by neutrophil elastase, chymotrypsin and trypsin. *FEBS Lett.* 351:85–89.

Kielty, C.M., E. Hanssen, and C.A. Shuttleworth. 1998. Purification of fibrillin-containing microfibrils and collagen VI microfibrils by density gradient centrifugation. *Anal. Biochem.* 255:108–112.

Loeys, B.L., J. Chen, E.R. Neptune, D.P. Judge, M. Podowski, T. Holm, J. Meyers, C.C. Leitch, N. Katsanis, N. Sharifi, et al. 2005. A syndrome of altered cardiovascular, craniofacial, neurocognitive and skeletal development caused by mutations in TGFßR1 or TGFßR2. *Nat. Genet.* 37:275–281.

Loeys, B.L., U. Schwarze, T. Holm, B.L. Callewaert, G.H. Thomas, H. Pannu, J.F. De Backer, G.L. Oswald, S. Symoens, S. Manouvrier, et al. 2006. Aneurysm syndromes caused by mutations in the TGF-beta receptor. *N. Engl. J. Med.* 355:788–798.

Marson, A., M.J. Rock, S.A. Cain, L.J. Freeman, A. Morgan, K. Mellody, C.A. Shuttleworth, C. Baldock, and C.M. Kielty. 2005. Homotypic fibrillin-1 interactions in microfibril assembly. *J. Biol. Chem.* 280:5013–5021.

Maslen, C.L., G.M. Corson, B.K. Maddox, R.W. Glanville, and L.Y. Sakai. 1991. Partial sequence of a candidate gene for the Marfan syndrome. *Nature*. 352:334–337.

Matsumoto, N., E. Ishimura, H. Koyama, S. Tanaka, Y. Imanishi, A. Shioi, M. Inaba, and Y. Nishizawa. 2003. Blocking of alpha 5 integrin stimulates production of TGF-beta and PAI-1 by human mesangial cells. *Biochem. Biophys. Res. Commun.* 305:815–819.

Matyas, G., E. Arnold, T. Carrel, D. Baumgartner, C. Boileau, W. Berger, and B. Steinmann. 2006. Identification and in silico analyses of novel TGFBR1 and TGFBR2 mutations in Marfan syndrome-related disorders. *Hum. Mutat.* 27:760–769.

Menon, R.P., M.R. Menon, X. Shi-Wen, E. Renzoni, G. Bou-Gharios, C.M. Black, and D.J. Abraham. 2006. Hammerhead ribozyme-mediated silencing of the mutant fibrillin-1 of tight skin mouse: insight into the functional role of mutant fibrillin-1. *Exp. Cell Res.* 312:1463–1474.

Mizuguchi, T., G. Collod-Beroud, T. Akiyama, M. Abifadel, N. Harada, T. Morisaki, D. Allard, M. Varret, M. Claustres, H. Morisaki, et al. 2004. Heterozygous TGFßR2 mutations in Marfan syndrome. *Nat. Genet.* 36:855–860.

Mould, A.P., S.K. Akiyama, and M.J. Humphries. 1995. Regulation of integrin alpha 5 beta 1-fibronectin interactions by divalent cations. Evidence for distinct classes of binding sites for Mn^{2+}, Mg^{2+}, and Ca^{2+}. *J. Biol. Chem.* 270:26270–26277.

Munger, J.S., J.G. Hapel, P.E. Gleizes, R. Mazzieri, I. Nunes, and D.B. Rifkin. 1997. Latent transforming growth factor-beta: structural features and mechanisms of activation. *Kidney Int.* 51:1376–1382.

Neptune, E.R., P.A. Frischmeyer, D.E. Arking, L. Myers, T.E. Bunton, B. Gayraud, F. Ramirez, L.Y. Sakai, and H.C. Dietz. 2003. Dysregulation of TGF-beta activation contributes to pathogenesis in Marfan syndrome. *Nat. Genet.* 33:407–411.

Ng, C.M., A. Cheng, L.A. Myers, F. Martinez-Murillo, C. Jie, D. Bedja, K.L. Gabrielson, J.M. Hausladen, R.P. Mecham, D.P. Judge, and H.C. Dietz. 2004. TGF-beta-dependent pathogenesis of mitral valve prolapse in a mouse model of Marfan syndrome. *J. Clin. Invest.* 114:1586–1592.

Pereira, L., M. D'Alessio, F. Ramirez, J.R. Lynch, B. Sykes, T. Pangilinan, and J. Bonadio. 1993. Genomic organization of the sequence coding for fibrillin, the defective gene product in Marfan syndrome. *Hum. Mol. Genet.* 2:961–968.

Perkins, D.N., D.J. Pappin, D.M. Creasy, and J.S. Cottrell. 1999. Probability-based protein identification by searching sequence databases using mass spectrometry data. *Electrophoresis*. 20:3551–3567.

Ramirez, F., L.Y. Sakai, H.C. Dietz, and D.B. Rifkin. 2004. Fibrillin microfibrils: multipurpose extracellular networks in organismal physiology. *Physiol. Genomics*. 19:151–154.

Reinhardt, D.P., D.R. Keene, G.M. Corson, E. Poschl, H.P. Bachinger, J.E. Gambee, and L.Y. Sakai. 1996. Fibrillin-1: organization in microfibrils and structural properties. *J. Mol. Biol.* 258:104–116.

Reinhardt, D.P., J.E. Gambee, R.N. Ono, H.P. Bachinger, and L.Y. Sakai. 2000a. Initial steps in assembly of microfibrils. Formation of disulfide-cross-linked multimers containing fibrillin-1. *J. Biol. Chem.* 275:2205–2210.

Reinhardt, D.P., R.N. Ono, H. Notbohm, P.K. Muller, H.P. Bachinger, and L.Y. Sakai. 2000b. Mutations in calcium-binding epidermal growth factor modules render fibrillin-1 susceptible to proteolysis. A potential disease-causing mechanism in Marfan syndrome. *J. Biol. Chem.* 275:12339–12345.

Rifkin, D.B. 2005. Latent transforming growth factor-beta (TGF-beta) binding proteins: orchestrators of TGF-beta availability. *J. Biol. Chem.* 280:7409–7412.

Robinson, P.N., E. Arteaga-Solis, C. Baldock, G. Collod-Beroud, P. Booms, A. De Paepe, H.C. Dietz, G. Guo, P.A. Handford, D.P. Judge, et al. 2006. The molecular genetics of Marfan syndrome and related disorders. *J. Med. Genet.* 43:769–787.

Rock, M.J., S.A. Cain, L.J. Freeman, A. Morgan, K. Mellody, A. Marson, C.A. Shuttleworth, A.S. Weiss, and C.M. Kielty. 2004. Molecular basis of elastic fiber formation. Critical interactions and a tropoelastin-fibrillin-1 cross-link. *J. Biol. Chem.* 279:23748–23758.

Sawyer, J.S., B.D. Anderson, D.W. Beight, R.M. Campbell, M.L. Jones, D.K. Herron, J.W. Lampe, J.R. McCowan, W.T. McMillen, N. Mort, et al. 2003. Synthesis and activity of new aryl- and heteroaryl-substituted pyrazole inhibitors of the transforming growth factor-beta type I receptor kinase domain. *J. Med. Chem.* 46:3953–3956.

Schultz-Cherry, S., S. Ribeiro, L. Gentry, and J.E. Murphy-Ullrich. 1994. Thrombospondin binds and activates the small and large forms of latent transforming growth factor-beta in a chemically defined system. *J. Biol. Chem.* 269:26775–26782.

Sherratt, M.J., D.F. Holmes, C.A. Shuttleworth, and C.M. Kielty. 2004. Substrate-dependent morphology of supramolecular assemblies: fibrillin and type-VI collagen microfibrils. *Biophys. J.* 86:3211–3222.

Shi, Y., and J. Massague. 2003. Mechanisms of TGF-beta signaling from cell membrane to the nucleus. *Cell*. 113:685–700.

Singh, K.K., K. Rommel, A. Mishra, M. Karck, A. Haverich, J. Schmidtke, and M. Arslan-Kirchner. 2006. TGFBR1 and TGFBR2 mutations in patients with features of Marfan syndrome and Loeys-Dietz syndrome. *Hum. Mutat.* 27:770–777.

Sinha, S., C. Nevett, C.A. Shuttleworth, and C.M. Kielty. 1998. Cellular and extracellular biology of the latent transforming growth factor-beta binding proteins. *Matrix Biol.* 17:529–545.

Siracusa, L.D., R. McGrath, Q. Ma, J.J. Moskow, J. Manne, P.J. Christner, A.M. Buchberg, and S.A. Jimenez. 1996. A tandem duplication within the fibrillin 1 gene is associated with the mouse tight skin mutation. *Genome Res.* 6:300–313.

Suk, J.Y., S. Jensen, A. McGettrick, A.C. Willis, P. Whiteman, C. Redfield, and P.A. Handford. 2004. Structural consequences of cysteine substitutions C1977Y and C1977R in calcium-binding epidermal growth factor-like domain 30 of human fibrillin-1. *J. Biol. Chem.* 279:51258–51265.

Vollbrandt, T., K. Tiedemann, E. El-Hallous, G. Lin, J. Brinckmann, H. John, B. Batge, H. Notbohm, and D.P. Reinhardt. 2004. Consequences of cysteine mutations in calcium-binding epidermal growth factor modules of fibrillin-1. *J. Biol. Chem.* 279:32924–32931.

Young, G.D., and J.E. Murphy-Ullrich. 2004. Molecular interactions that confer latency to transforming growth factor-beta. *J. Biol. Chem.* 279:38032–38039.

Zhou, X., F.K. Tan, D.M. Milewicz, X. Guo, C.A. Bona, and F.C. Arnett. 2005. Autoantibodies to fibrillin-1 activate normal human fibroblasts in culture through the TGF-beta pathway to recapitulate the "scleroderma phenotype". *J. Immunol.* 175:4555–4560.